

Aerodynamic impact of cycling postures on drafting in single paceline configurations

Thijs van Druenen ^{a,*}, Bert Blocken ^{a,b}

^a Building Physics and Services, Department of the Built Environment, Eindhoven University of Technology, P.O. box 513, 5600 MB, Eindhoven, the Netherlands

^b Building Physics and Sustainable Design, Department of Civil Engineering, KU Leuven, Kasteelpark Arenberg 40 - bus 2447, Leuven 3001, Belgium



ARTICLE INFO

Keywords:

Cycling aerodynamics
Drafting
Drag reduction
Computational fluid dynamics (CFD)
Wind tunnel measurements

ABSTRACT

This paper presents finite-volume-based scale-adaptive simulations of single paceline configurations up to eight cyclists for three different postures. In cycling, drag reduction by drafting in pacelines is a key strategy to limit energy expenditure. The drag reductions of individual cyclists and of the paceline as a whole are determined by several factors, including cycling posture. To the best of our knowledge, a systematic study on the effect of cyclist posture on the drag in single pacelines has not yet been published in the scientific literature. In this study, drag reduction and flow field data were computed while validation was performed by wind tunnel measurements. The three investigated postures concern a road race dropped posture with either a large or small sagittal torso angle and a time trial posture. For the considered pacelines in which all cyclists have the same posture, the drag of a cyclist could be reduced by changing either the posture, or the position, or both. Changing posture can yield a maximum drag reduction of about 15% for the leading cyclist. The position in the paceline with minimum drag was the one but last, independent of the investigated cycling postures. For the pacelines containing eight cyclists, maximum drag reductions up to 63% were found. The largest drag reduction was 68%, obtained by riding in penultimate position in an eight cyclist paceline in dropped position with a small sagittal torso angle.

Nomenclature

A	frontal area
Awake	cross-sectional area of the core of the wake
CCURV	curvature correction coefficient
C_D	drag coefficient
C_{DA}	drag area
CFD	computational fluid dynamics
CFL	courant-friedrichs-Lowy number
DES	Detached-Eddy simulation
DP	road race dropped posture
DP-high	road race dropped posture with high sagittal torso angle
DP-low	road race dropped posture with low sagittal torso angle
FVM	finite volume method
k_s	equivalent sand-grain roughness height
K_s^+	dimensionless roughness height
LBM	lattice Boltzmann method
LES	Large-Eddy simulation
RANS	Reynolds-averaged Navier-Stokes
SAS	scale-adaptive simulation

SST	shear stress transport turbulence model
TSST	transition shear stress transport turbulence model
TPP	time trial posture
TTT	team time trial
U	streamwise velocity
UP	road race upright posture
u^*	friction velocity
WT	wind tunnel
y_p	normal distance of the cell center point to the wall surface
y^+	dimensionless wall unit
Δt	time step size
Δx	streamwise cell size
ν	kinematic viscosity

1. Introduction

Saving on energy expenditure by drafting is omnipresent in nature. Many species travel in well organized groups. In groups of flying birds and schools of fish, the purpose of traveling in a formation is to reduce energy expenditure. Weimerskirch et al. [1] estimated by means of heart

* Corresponding author.

E-mail address: t.v.druenen@tue.nl (T. van Druenen).

rate measurements that pelicans reach energy savings in the range of 11 to 14% by flying in 'V' formation. Marras et al. [2] found energy savings up to 19.4% for fish swimming in schools. Also in human transport, energy expenditure is reduced by drafting. Platooning of trucks [3–5], cars [5–7] and trains [8,9], moving closely together, reduces fuel consumption and emissions as it reduces the aerodynamic drag of all vehicles in the platoon.

Also in sports where much athlete's energy expenditure is attributed to overcoming drag, drafting can be an essential strategy. This is the case with running [10,11], swimming [12,13], skiing [14,15] and speed skating [16,17]. A unique type of drafting is present in tandem cycling [18–21]. By drafting in very close proximity the front and rear tandem athlete can achieve drag reductions of 15 and 58% respectively [19] compared to an isolated cyclist. Drafting is also a common strategy in conventional cycling. At professional racing speeds of about 40 km/h on flat terrain, the aerodynamic resistance or drag is about 90% of the total resistance [22–24]. The greatest potential of saving energy for a cyclist therefore lies in its aerodynamics [25]. Since drag reductions up to 95% by drafting [26] have been reported in the literature, drafting is a key element in a cycling race.

In cycling, a distinction can be made between two types of drafting configurations: pelotons and pacelines. The peloton is the main group of cyclists in a race, where usually several cyclists ride side-by-side, and where there is some form of rotation of cyclists in the front of the group (see Fig. 1a). In general, only a limited number of cyclists take turns riding at front, while the majority does not participate and rides further downstream in the formation to conserve energy expenditure. Peloton configurations are a common phenomenon in regular road races in cycling. Wind tunnel (WT) tests and computational fluid dynamics (CFD) simulations have shown that drag reductions of up to 95% can be achieved in the middle of a tightly packed peloton [26].

In paceline configurations, generally every cyclist in the group participates in riding at the front, although there may be exceptions. Here, cyclists alternately take the lead while other group members take advantage of the slipstream behind the leading cyclist. After its turn, the leading cyclist will generally line up at the very end of the formation (see Fig. 1b). The second cyclist takes over and the former leading cyclist can recover from its effort. In regular road races, paceline configurations are observed in breakaways, where cyclists join forces to break out of the peloton, and in sprint preparations. Here, a paceline is formed with the best sprinter of the team at the end of the formation. The team sets a fast pace to keep their sprinter at the front of the race, discourage late attacks, and allow the sprinter to launch his or her sprint as late as possible with the least amount of energy spent before this particular moment. Also in a team time trial (TTT), a road cycling race in which cyclists of the same team race against the clock and try to complete the course in the fastest time, cycling in paceline formations is the main strategy. Typical TTTs can contain 6 to 9 cyclists.

The most commonly used paceline formations are the single and circular paceline [27]. Most studies on drafting in cycling were conducted for the single paceline with the cyclists in a time trial posture (TTP). These studies reported that the drag of the trailing cyclist(s) is greatly reduced [28–34], but also that the leading cyclist benefits from riding in a single paceline with reported drag reductions of 2.6% (excluding bicycle) [28], 3% [29] and 5% [30,31]. Drag reductions of about 49% [31] and, depending on wheel-to-wheel distance, between 36 and 19% [29] were found for the trailing cyclist for single pacelines of two cyclists in TTP. For single pacelines with four cyclists in TTP, drag reductions up to about 38% [35], 40% (excluding bicycle, [33]) and 57% [34] were found. Blocken et al. [29] performed CFD simulations for TTT pacelines up to 9 cyclists and found a maximum drag reduction of 60.3% for the cyclist in seventh position in a TTT paceline with nine cyclists. To avoid confusion, in the present study the term posture is used to define the geometry of the cyclist's body on the bicycle, while the term position refers to the location of the cyclist in the paceline.

The forementioned studies are concerned with drafting in a single paceline in TTP configuration. Mainly, these studies were conducted with the inclusion of an aerodynamically designed time trial bicycle, a closed rear disk wheel and aerodynamic helmet, as seen in TTT events. In regular road races it is not allowed to use this equipment and instead the cyclist rides a road race bicycle with spoked wheels and wears a regular helmet. As a consequence, the cyclist's posture in regular road races is generally less aerodynamic compared to the TTP. In the upright posture (UP) the cyclist has his hands on top of the handlebars. In general, this is the preferred posture in terms of comfort. To improve their aerodynamics cyclists usually adopt a dropped posture (DP), in which cyclists have their hands gripping in the lower portion of the handlebars, reducing their sagittal torso angle. Studies by WT testing or CFD simulations on the effect of drafting in regular road race postures are scarce. Zdravkovich et al. [36] and Belloli et al. [37] performed WT tests on two drafting road cyclists in UP and found a drag reduction for the trailing cyclist of 49% and 45% respectively at 0.1 m streamwise separation. A systematic CFD analysis up to 8 drafting road cyclists on a race bicycle in DP was carried out by van Druenen et al. [38]. However, because this study involved drafting in uphill sections of the race, the evaluated cycling speeds were much lower compared to those in flat-terrain breakaways or sprint trains and only the single DP posture was evaluated. Early coast down tests reported energy expenditures of 27% [39] and power production reductions of 35% [35] for single pacelines containing four cyclists in DP, while a maximum energy expenditure reduction of 39% was found in the back of an eight cyclist single paceline [39]. Edwards and Byrnes [40] performed power measurements on single pacelines of two cyclists in DP and found power reductions of about 33% for the trailing cyclist.

The drag reductions that can be achieved by drafting depend on several factors. An important factor is the streamwise wheel-to-wheel

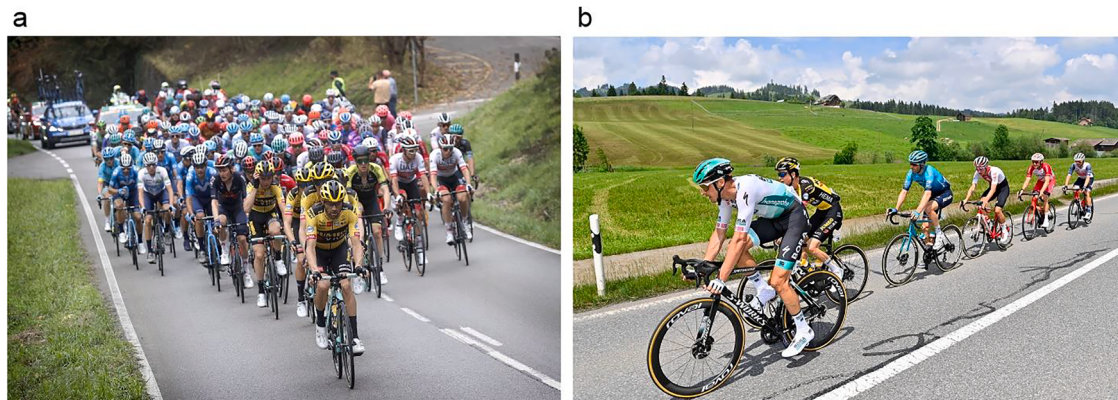


Fig. 1. Drafting configurations in regular road races. (a) Peloton and (b) single paceline (Source: Cor Vos Agency, reproduced with permission).

separation distance. Several studies showed that the drag reduction for all cyclists in a paceline grows with decreasing streamwise separation distance [29,35–37,41]. Morphological factors and the posture of the athlete on the bicycle also play an important role. It was found that the drag reduction by drafting increased with a larger drag area of the leading cyclist [35,40]. Barry et al. [34] performed WT measurements on a team of four time trial cyclists in TTP. Strong aerodynamic interactions were observed that differed significantly between the cyclists and appeared to be a function of the body shape. Defraeye et al. [33] performed CFD simulations on the influence of cyclist posture on the drag for four drafting cyclists and found variations in individual and total drag. Individual differences in posture and the different sequences of cyclists led to variation of drag reduction for the individual cyclists and for the total drag of the group. More information on previous research on drafting in cycling can be found in review papers [42–44].

While these studies confirmed the impact of the athlete's posture on the individual and total drag, to the best of our knowledge, a systematic study on the effect of cyclist posture on the drag in single pacelines has not yet been published in the scientific literature. Potential methods to assess drag in cycling pacelines as a function of cycling posture are described by Debraux et al. [45]. Ranging from less (coast-down methods) to more (linear regression analysis in combination with power meters) reliable approaches, field methods can provide drag measurements in actual race conditions. However, meteorological conditions and the nature of the road can potentially induce errors. Moreover, it is difficult to conduct systematic field studies and isolate the posture variable, since ideally identical cyclists are desired at every position in the paceline. The latter could be solved by implementing (scaled) cyclist models in a wind tunnel study. Because of its validity and reliability, the wind tunnel is considered as the reference technique for assessing aerodynamic drag [45,46].

For cross-comparison of results, and to gain more insight into the flow field around the paceline formation, CFD simulations could be a valuable additional method. CFD is well suited for systematic studies and allows evaluation of the drag with high sensitivity [45]. Most CFD work in cycling aerodynamics is based on finite volume methods (FVM). It maintains conservation of mass and momentum, has shown good validation results and it is less prone to mesh type and mesh quality compared to finite element methods [47]. It is also stated to be faster and the memory requirements are lower [48]. In addition, some main open-source and commercial CFD software packages are FVM-based [47,49,50]. Regarding the application of FVM-based CFD simulation to bluff body aerodynamics, the Reynolds-averaged Navier-Stokes (RANS) approach is most commonly used because of its computational efficiency [51]. Most of the aforementioned studies on the assessment of drag in sport or automotive flows applied the shear stress transport (SST) $k-\omega$ turbulence model [52] [e.g. 10,11,18–20] or the standard $k-e$ turbulence model [53] [e.g. 28,29,33] for closure of the 3D steady RANS equations. More recently, several studies have applied the transition shear stress transport (TSST) turbulence model [54,55,26,56] for closure and showed good agreement with wind tunnel measurements.

While Large-Eddy simulation (LES) has not often been used in simulations of cycling aerodynamics, the application of hybrid models and its ability to resolve turbulent scales wake has shown promising results [7,9,57–59]. A common example is Detached-Eddy simulation (DES), which is a blend of RANS and LES models, where RANS is used to approximate the boundary layer and LES is used to capture the time-varying flow away from boundaries. DES is highly grid sensitive and results can suffer from modeled stress depletion and grid-induced separation [60]. Although these issues have been gradually addressed through improvements to the model, scale adaptive simulation (SAS) could be a safer option for scale-resolving simulation given the complex geometries in the current study. SAS is able to resolve part of the turbulence spectrum for unstable flows depending on the cell size and time step. It shows a gradual transition from Unsteady RANS-type to LES-type behavior as the temporal and spatial resolution are increased. Unlike

problems with LES or DES caused by insufficient grid or time resolution, SAS employs URANS as a back-up on coarse grids or time steps [61]. A known constraint is that the scale-resolving mode is only activated if the flow is sufficiently unstable. In cyclist aerodynamics however, the wake is highly turbulent. Examples of the application of SAS, coupled with the SST $k-\omega$ model [52], in cycling aerodynamics are given by Blocken et al. [62] and van Druenen et al. [38]. Unsteady methods such as LES, DES and SAS are much more computationally demanding than RANS. In this perspective, the application of Lattice-Boltzmann methods (LBM) is worth mentioning. Evaluation of computational methods on the assessment of drag on automotive models [63] showed an improved prediction of LBM compared to RANS. Moreover, while URANS and DES required 50 to 250 times the computational cost of steady RANS, this was only 5 to 10 for LBM, making the latter a potential alternative to unsteady FVM-based methods. However, no publications or best practice guidelines were found on the application of LBM to cycling aerodynamics.

In the present study, drag reductions and flow field data were obtained by FVM-based CFD simulations for various postures in single pacelines up to eight cyclists. The performance of two turbulence-modeling methods (TSST vs. SAS) was assessed and validation of both methods was performed by WT measurements. Three postures were investigated: a road race dropped posture with large sagittal torso angle (DP-high); a road race dropped posture with small sagittal torso angle (DP-low); and a time trial posture (TTP).

2. Cycling postures

The three examined postures are depicted in Fig. 2, together with the frontal area A and the six characteristic angles specifying the cyclist's posture on the bicycle. The postures DP-high ($A = 0.440 \text{ m}^2$) and DP-low ($A = 0.391 \text{ m}^2$) are common in regular road races. A road race bicycle, spoked wheels and a regular helmet are included. DP-high and DP-low are observed in paceline configurations in breakaways and sprint trains. The TTP ($A = 0.311 \text{ m}^2$) includes a TT bicycle and TT helmet as well as a tri-spoke front wheel and closed rear disk wheel. TTP is used in individual and team time trials. It was included here as a benchmark because a similar study exists for time-trial configurations [29]. The cyclist and bicycle geometries were obtained by 3D scanning using an Eva structured 3D light scanner [64]. The procedure of processing the body geometry and reporting the results was approved by the ethical board committee of Eindhoven University of Technology with reference code (ERB2020BE 1,859,456 WT). The cyclist had a height of 1.83 m and a weight of 72 kg. Saddle height was 0.92 m. The bicycle geometry was simplified, e.g. chains, sprockets, gear mechanisms etc. were not included as they were considered small enough not to significantly influence the results. Wheels were not rotating and the cyclist was not pedaling.

3. Wind tunnel measurements

WT measurements were performed for the DP-high posture in the closed circuit WT at Eindhoven University of Technology in the Netherlands [65]. The impact of boundary layer development was mitigated by placing the cyclist models on an elevated sharp-edged platform with integrated force transducer (see Fig. 3). The models were cast at quarter-scale with a frontal area of 0.027 m^2 . The cross-section of the WT test section was $(w \times h) 3 \times 2 \text{ m}^2$. Considering the part of the cross-section above the platform yielded a blockage ratio of 0.7%. This was well below the recommended maximum of 5% [66]. The reduced-scale wheel-to-wheel separation distance between the cyclists in the WT tests was 0.0375 m (full scale = 0.15 m). A force transducer designed for quarter-scale cycling test with an accuracy of 0.001 N was used and placed alternately below each cyclist in the paceline.

The measurements were performed for pacelines of two, three and

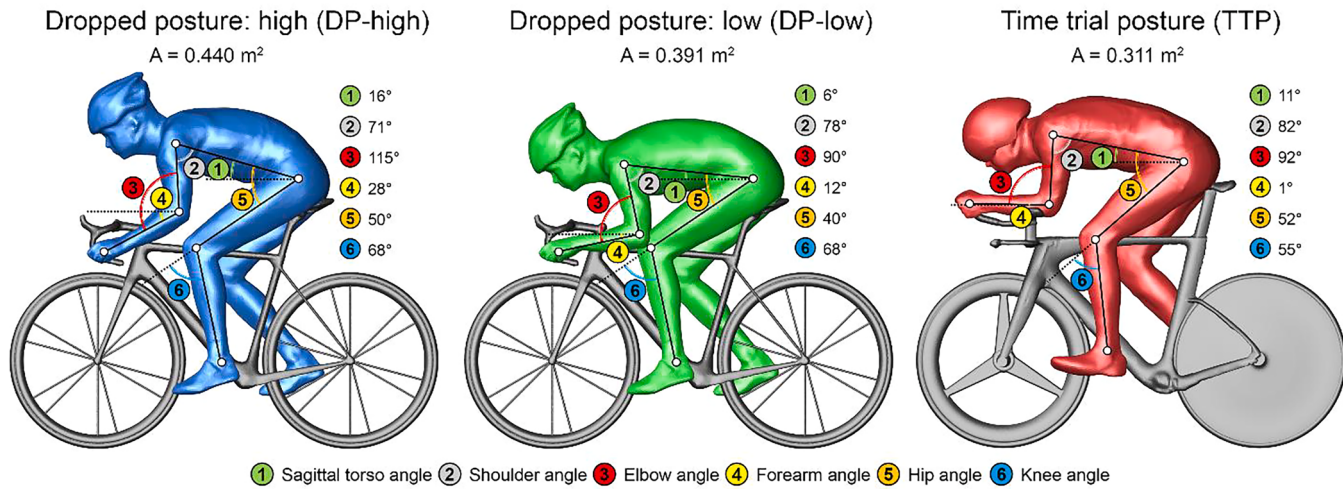


Fig. 2. The three cycling postures with definition, frontal area A and values of (1) sagittal torso angle, (2) shoulder angle, (3) elbow angle, (4) forearm angle, (5) hip angle, (6) knee angle.

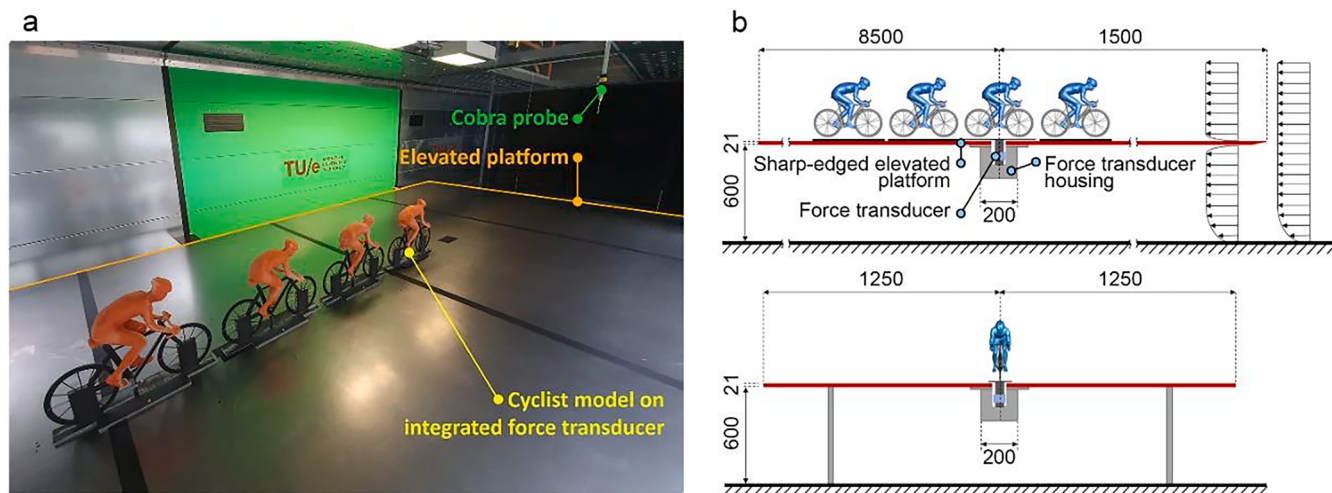


Fig. 3. Wind tunnel set-up. Dimensions in mm.

four cyclists, with a speed of 25 m/s. This is close to the maximum wind speed inside the tunnel for this particular configuration. The boundary layer height at the measurement position was 35 mm, which was lower than the cyclist's feet and pedals. The models were manufactured with a rather high geometric surface roughness of 0.25 mm to enhance Reynolds number independence [26]. Reynolds independence was tested and the results are shown in Fig. 4. For the first, third and fourth cyclist Reynolds independence was achieved at 20 m/s. An exception was the second cyclist. Since the maximum speed has been reached, the graph does not show convergence yet. Air temperature, atmospheric pressure, humidity and free wind speed were recorded during the measurements. The latter was measured with a cobra probe and the turbulence intensity was about 0.5% at the position of the first cyclist. The drag force results were adjusted to match conditions of 15 °C at 0 m height and standard atmospheric pressure 101,325 Pa, as also applied in the CFD simulations.

4. CFD simulations: validation

4.1. Approximate form of governing equations and solver settings

The FVM-based CFD simulations were performed using the

commercial CFD code ANSYS Fluent 19.2 [49] on the Dutch national supercomputer Cartesius. Simulations were performed on up to 16 nodes of Intel® Xeon® CUP E5-2690 v3 (Haswell 24 core at 2.60 GHz) with 64 GB RAM each. The performance of two turbulence-modelling methods was assessed in the validation study. The first method applied 3D steady RANS equations with the TSST turbulence model for closure [54,55]. This turbulence model is based on the coupling of the SST $k-\omega$ transport equations with two additional transport equations to track the intermittency and transition onset criteria. The second, computationally more expensive URANS-LES approach, was scale-adaptive simulation (SAS) [61,67] coupled with the SST $k-\omega$ model [52].

The TSST model was applied with roughness correlation, curvature correction with $C_{CURV} = 1$ and production limiters with clip factor 10 [49]. Pressure-velocity coupling was performed by the Coupled scheme. Pressure interpolation was second order. For both the convection and the viscous terms of the governing equations second-order upwind discretization schemes were used. The gradients were computed with the Green-Gauss node-based scheme. To stabilize the simulations and improve convergence, pseudo-transient under-relaxation was applied. A minimum of 10,000 pseudo-transient time steps with a pseudo-time step size of 0.01 s were used. Averaged drag values were obtained by averaging over the last 9000 time steps.

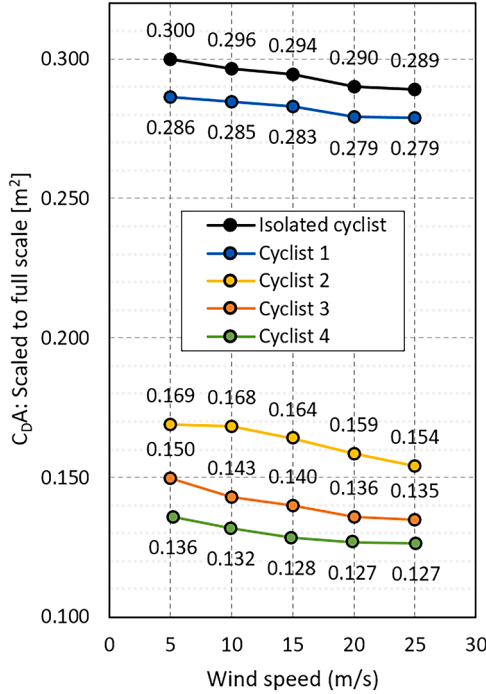


Fig. 4. Results of wind tunnel Reynolds independence tests for the isolated cyclist and four cyclists paceline.

For the SAS approach pressure-velocity coupling was taken care of by the PISO scheme. Curvature correction with $C_{\text{CURV}} = 1$ and production limiters with clip factor 10 were applied [49]. Pressure-interpolation was second order. Bounded central differencing was used for the momentum equation and second-order upwind discretization schemes were used for turbulent kinetic energy and specific dissipation rate. In the

absence of a subgrid-scale model, higher-order schemes could produce more accurate results on coarser grids, at the same computational cost [68]. Nevertheless, schemes and solver settings applied in this study were based on best practice guidelines specific to SAS [69]. Gradient interpolation was performed by the Green-Gauss node based scheme. The time step size was determined by keeping the Courant-Friedrichs-Lowy (CFL) number below one in the regions between the cyclists. The CFL number relates the size of the time step Δt to the streamwise cell size Δx and streamwise velocity U as $\text{CFL} = U\Delta t/\Delta x$, with $U = 15 \text{ m/s}$ and $\Delta x = 0.03 \text{ m}$ in the region between the cyclists. Based on a conservative choice of $\text{CFL} = 0.5$, the SAS simulations were conducted with a time step of $\Delta t = 0.001 \text{ s}$. After an initialization phase of 1000 timesteps, 5000 time steps were required to obtain a constant moving average of the sampled drag area for all cyclists in the paceline.

4.2. Computational domain and grid

The simulations were performed at full scale. For all configurations, the computational domain had dimensions ($L \times W \times H$) $54.5 \times 17.5 \times 18 \text{ m}^3$ (see Fig. 5a), according to best practice guidelines [70–72]. Streamwise dimensions were based on the configuration with eight cyclists. The associated computational grid for the DP-low eight cyclists paceline of 173,713,019 cells is shown in Fig. 5b, for which a detail of the region of interest is given in Fig. 5c. The grids were selected based on grid-sensitivity analyses (Section 4.4).

4.3. Boundary conditions

At the inlet of the computational domain a uniform mean velocity of 15 m/s and a turbulence intensity of 0.5% was imposed, which represents high-speed cycling without external (atmospheric) wind. An equivalent sand-grain roughness height of $k_s = 0.1 \text{ mm}$ was applied to the cyclist's body surfaces [26,38,62], while the bicycle surfaces were modeled as smooth no-slip walls. Zero static gage pressure was specified at the outlet. The slip wall boundary condition was applied to the

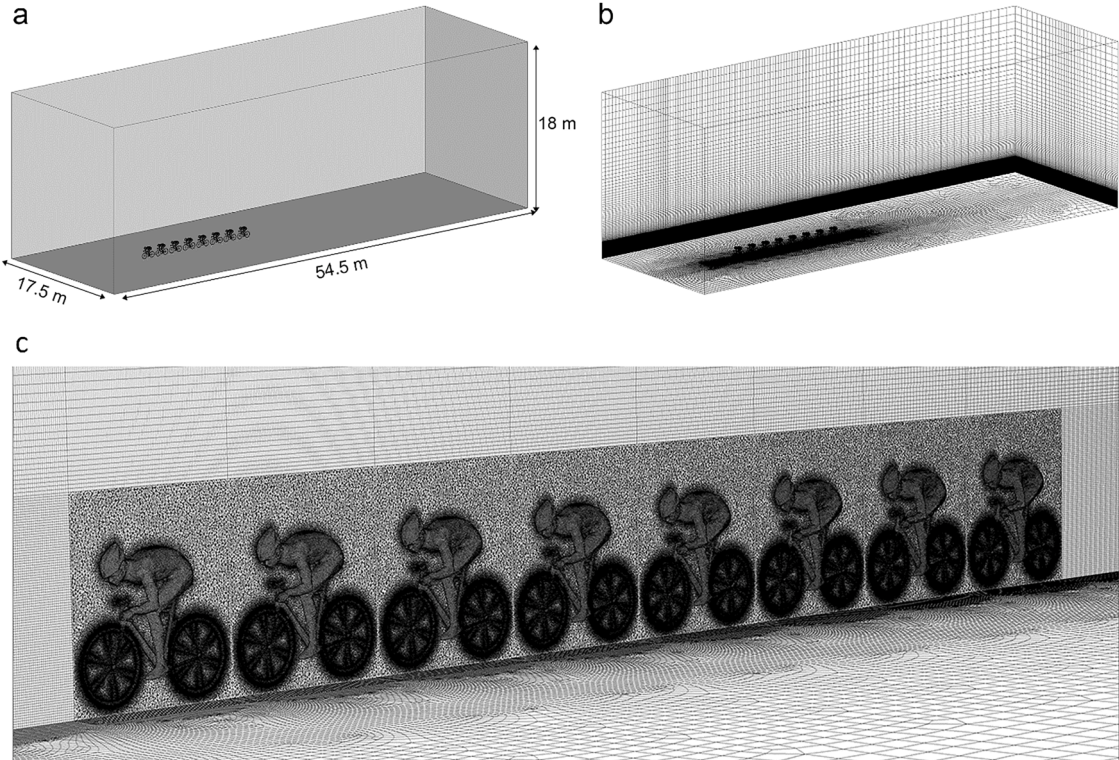


Fig. 5. Computational (a) domain, (b) grid (173,713,019 cells) and (c) grid detail for the DP-low 8 cyclists paceline.

bottom, top and lateral boundaries.

4.4. Grid-sensitivity analyses

Grid-sensitivity analyses were performed for both the TSST and SAS methods. Three hybrid hexahedral-tetrahedral grids of 25,621,919, 35,248,553 (see Fig. 6a) and 49,111,825 cells were constructed for the isolated cyclist configuration. Table 1 presents the grid characteristics of the three grids, in which the surface, volume and boundary-layer cells were systematically refined. To resolve the thin viscous sublayer of the boundary layer at the surface, the normal distance of the cell center point from the wall surface y_p was determined so that y^+ is lower than 1. The dimensionless wall unit y^+ is defined by $y^+ = u^* y_p / \nu$ where u^* is the friction velocity and ν is the local kinematic viscosity. Area-weighted average y^+ values are reported in Table 2. The higher y^+ values for the body surfaces are due to the application of roughness. As k_s is larger than y_p , the wall is virtually shifted to half the height of the roughness element so that $y^+ = y^+ + K_s^+ / 2$ with K_s^+ the non-dimensional roughness height $K_s^+ = k_s u^* / \nu$ [49].

The results were evaluated in terms of the drag area $C_D A$, which is the product of the frontal area A and the drag coefficient C_D and presented in Fig. 6b. The results obtained on the coarse grid showed a difference of 1.4% and 3.1% compared to those on the fine grid for respectively the TSST (0.281 vs. 0.277 m²) and SAS (0.260 vs. 0.268 m²) method. The use of the medium grid resulted in an underestimation of 0.7% compared to the use of the fine grid for both the TSST (0.275 vs. 0.277 m²) and SAS (0.266 vs. 0.268 m²) method. Based on a trade-off between accuracy and computational demand the medium grid (Fig. 6a) was retained for the remainder of this study.

4.5. Results

The results of the validation study were evaluated in terms of percentage drag of that of an isolated cyclist at equal speed and are shown for both the WT measurements and CFD simulations in Fig. 7. Drag reductions were observed for all cyclists in the paceline. The smallest reduction was found for the leading cyclist (C1) and the drag reduction increased for cyclists further down the paceline. This trend was observed for both the WT measurements and the CFD simulations. Compared to using the TSST turbulence model, the results obtained with the SAS method showed an equal or better agreement with the WT measurement for C1, C3 and C4. The SAS method overestimated the drag for C2 in all configurations. Here, the use of the TSST turbulence model showed a better agreement. With a mean error of 2.1%, both methods were fairly consistent with the WT measurements. Though requiring significantly

Table 1
Grid characteristics.

Resolution	Surface cell size	Outer volume cell size	y_p	Prism layers	Cells
Coarse	3 – 8 mm	40 mm	0.0150 mm	30	25,621,919
Medium	2 – 5 mm	30 mm	0.0100 mm	40	35,248,553
Fine	2 – 3 mm	25 mm	0.0075 mm	45	49,111,825

Table 2
Area-weighted average y^+ values.

Resolution	Approach	Surface	y^+
Coarse	TSST	Bicycle	0.67
		Body	3.15
	SAS	Bicycle	0.69
		Body	3.35
Medium	TSST	Bicycle	0.45
		Body	2.96
	SAS	Bicycle	0.46
		Body	3.13
Fine	TSST	Bicycle	0.35
		Body	2.84
	SAS	Bicycle	0.35
		Body	3.05

more time, due to its better performance in wake regions [62] and taking into account pacelines up to eight cyclists, the SAS method was used for the rest of this study.

5. CFD simulations: parametric posture study

5.1. Computational settings and parameters

SAS simulations were performed for the three postures for configurations up to eight cyclists in a single paceline. The computational domain, grid, solver settings, schemes and boundary conditions were equal to those used in the validation study. The initialization phase consisted of 1000 timesteps per configuration, after which the number of required time steps to obtain a constant moving average of the drag values was different per configuration and ranged from 5000 for the isolated cyclists to 8000 for the eight cyclist configurations.

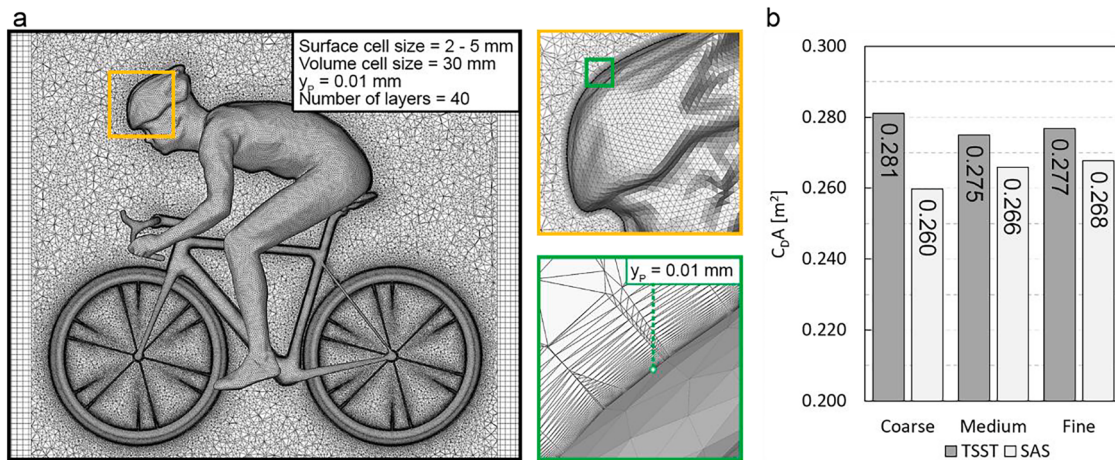


Fig. 6. (a) Computational medium-sized grid of 35,248,553 cells and (b) drag results for two computational methods and three grid refinements for the isolated cyclist.

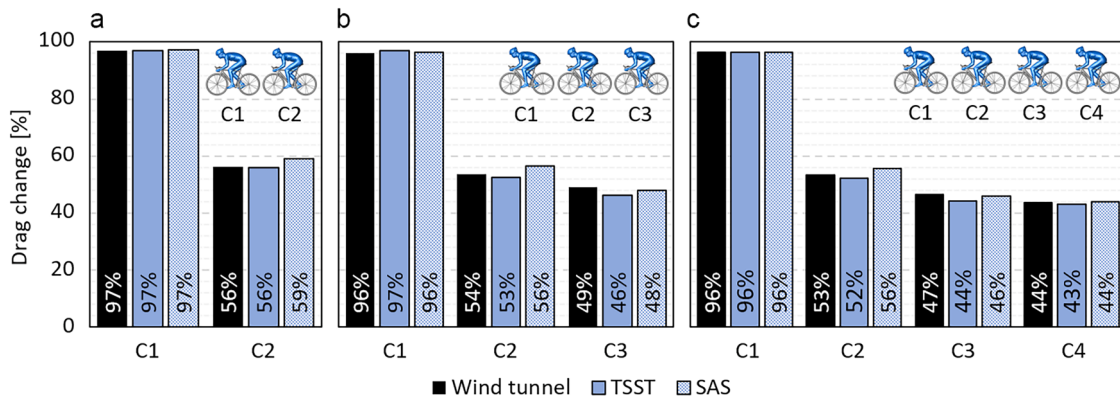


Fig. 7. Comparison of CFD and wind tunnel drag results for the (a) two, (b) three and (c) four cyclists configuration, as a percentage of the drag of an isolated cyclist.

5.2. Results

Fig. 8a provides the $C_D A$ values for every cyclist in pacelines in which all cyclists have the same posture. It is shown that the drag of a cyclist can be reduced by changing the posture, or the position in the paceline, or both. In general the highest $C_D A$ values were found for DP-high, while the cyclists in the TTP paceline experienced the lowest $C_D A$. For the isolated cyclist, $C_D A$ values of 0.266, 0.231 and 0.213 m^2 were calculated for DP-high, DP-low and TTP, respectively. As observed in previous studies, the drag on the leading cyclist decreased due to the other cyclists in its wake [28–31]. Blocken et al. [28,29] attributed this to the so-called subsonic upstream disturbance, resulting from the elliptical nature of the Navier-Stokes equations for subsonic flow. For pacelines of two to eight cyclists, the $C_D A$ of the leading cyclist was about 0.26 m^2 for DP-high, 0.22 m^2 for DP-low (-15% compared to DP-high) and 0.20 m^2 for TTP (-23% compared to DP-high). This difference in $C_D A$ between the postures reduces for positions further down the pacelines. For example, for the fifth cyclist in a single paceline of five cyclists, $C_D A$ values of 0.110, 0.104 (-5% compared to DP-high) and 0.097 m^2 (-12% compared to DP-high) were found for DP-high, DP-low and TTP respectively. For all postures the drag area reached a minimum for the last cyclist for pacelines up to five cyclists. For pacelines with six, seven and eight cyclists, the penultimate position was the position with the lowest $C_D A$.

Fig. 8b shows the percentage drag reduction where the reference (100%) is the isolated cyclist in the given posture. It indicates the drag reduction that can be obtained for a given posture, by changing the

position of the cyclist in the paceline. Overall, the change of drag was most pronounced for DP-high. This indicates that the aerodynamic interaction between the cyclists is most pronounced in the least aerodynamic posture. An exception to this was the drag change of the leading cyclist. For DP-high the drag reduction for the leading cyclist grew from 2.9% for two cyclists to 4.1% for eight cyclists in the paceline. For DP-low this increased from 4.5% to 4.9% and for TTP the drag reduction grew from 3.7% to 5.4% with increasing number of cyclists in the paceline. The largest drag reduction, as found in the penultimate position in the eight-cyclists paceline, was 63% for DP-high and 60% for both DP-Low and TTP.

Fig. 8c shows the percentage of drag reduction that results when the reference is the isolated cyclist in DP-high posture. For an isolated cyclist in DP-high, Fig. 8c indicates that a drag reduction of 13% could be obtained by changing posture to DP-low. In the event that the DP-low posture would be applied in a paceline of eight cyclists, the cyclist in penultimate position reduces its drag by 68% compared to riding solo in DP-high.

The mean drag area for pacelines up to eight cyclists is given in Table 3. For all postures the mean drag area decreases by the addition of cyclists to the paceline. As the number of cyclists in the paceline increases, the mean drag reduction per added cyclists becomes smaller. Compared to the isolated cyclist a mean drag area of about 60% was obtained for pacelines with four (DP-high) or five (DP-low and TTP) cyclists. In agreement with the drag change per cyclist (Fig. 8b), the drag change for the whole group was larger for less aerodynamic postures. Therefore, the reduction in mean drag was most pronounced for DP-

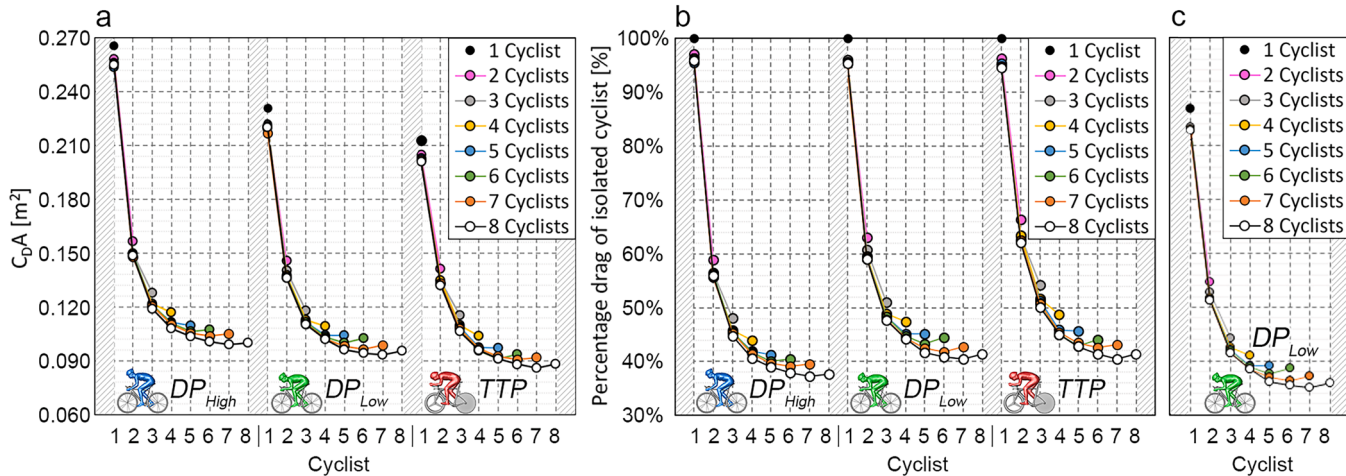


Fig. 8. Drag of every cyclist in configurations of up to 8 cyclists in terms of (a) $C_D A$, and as a percentage of the drag of the isolated cyclist in (b) the given posture and (c) DP-high posture.

Table 3
Mean drag area (m^2) of pacelines up to 8 cyclists.

	Mean drag area		
	DP-high	DP-low	TTP
1 Cyclist	0.266 (100%)	0.231 (100%)	0.213 (100%)
2 Cyclists	0.207 (78%)	0.184 (80%)	0.173 (81%)
3 Cyclists	0.178 (67%)	0.160 (69%)	0.150 (71%)
4 Cyclists	0.161 (60%)	0.145 (63%)	0.138 (65%)
5 Cyclists	0.149 (56%)	0.135 (59%)	0.128 (60%)
6 Cyclists	0.142 (53%)	0.129 (56%)	0.121 (57%)
7 Cyclists	0.135 (51%)	0.123 (53%)	0.116 (55%)
8 Cyclists	0.129 (49%)	0.118 (51%)	0.111 (52%)

high. For all postures the mean drag area for a paceline with 8 cyclists was about half that of the isolated cyclist.

Fig. 9 presents the contours of the mean static pressure coefficient for respectively the DP-high, DP-low and TTP configurations in the vertical centerplane and in an horizontal plane at 1 m height, for pacelines with one, four and eight cyclists. Figures for all pacelines are found in Appendix A. In general, areas of overpressure (red) are located in front of the cyclists and areas of underpressure (blue) behind them. The area of overpressure is smaller for postures with lower drag (Fig. 9a-c). Fig. 9 demonstrates the impact of the subsonic upstream disturbance on the leading cyclist in the paceline. A relatively large underpressure area is present behind the isolated cyclist (Fig. 9a-c). Because of the other cyclists in its wake, the underpressure area behind the leading cyclist is reduced in size and magnitude (Fig. 9d-i). Moreover, the last cyclist in the paceline experiences a larger underpressure area compared to all other cyclists in front of him/her, because the last cyclist does not have someone drafting behind its back. The largest overpressure area is visible in front of the leading cyclist. By drafting in the wake behind the leading cyclist, the trailing cyclists take shelter from the wind and the areas of overpressure in front of the trailing cyclists are reduced in size and magnitude.

Contours of mean velocity ratio are given in Fig. 10 for DP-high, DP-low and TTP, respectively. A similar trend was observed for all postures. The core of the wake that originates from the first cyclist grows further

downstream to about position four or five. From here, growth levels off and the cyclists further downstream the paceline experience similar drag benefits by drafting in the wake of those in front of them. This is more clearly demonstrated in Fig. 11, that displays the cross-sectional area of the core of the wake (A_{wake}) in a vertical plane, in which the core of the wake is described by mean velocity ratio < 0.5 . The velocity ratio is defined as the magnitude of the local 3D velocity vector divided by the cycling speed of 15 m/s. It confirms that the expansion of the core of the wake reduces further down the paceline.

For pacelines with four and eight cyclists a wider wake is visible for DP-high (Fig. 10d,g) compared to DP-low (Fig. 10e,h) and TTP (Fig. 10f, i). This observation is also confirmed by Fig. 11. The largest values for A_{wake} are found near position seven and eight in the eight cyclists paceline configurations. For DP-high the peak value for A_{wake} is about 0.42 m^2 , while lower peak values of about 0.38 m^2 and 0.36 m^2 are found for DP-low and TTP respectively.

To better understand the wake flow topology, instantaneous snapshots illustrated by isosurfaces of the q-criterion are given in Fig. 12. For the isolated cyclists (Fig. 12a,c,e) the predominant vortices were observed around the upper body of which the counter rotating hip/thigh vortices, as identified in the work of Crouch et al. [73], were the main wake structures. These complex loop-like structures were the result of the interaction between multiple streamlined coherent vortices originating from different parts of the body. For all postures large regions of separated flow were identified around the lower back, upper arms and lower and upper legs. Flow separation was also observed around the lower arms for DP-high (Fig. 12a). The separated flow of the arms interacted with the vortices around the side of the body and upper leg. This was most pronounced for the DP-low position (Fig. 12b). The lowest drag values for the isolated cyclists were found for TTP (see Fig. 8). This was reflected by the wake structures above the upper back area. While relatively small structures originated from the shoulder-region in TTP (Fig. 12e), large structures were observed in this region for both DP-high (Fig. 12a) and DP-low (Fig. 12c) as they interacted with large separated flow from the regular helmet. Compared to the spoked wheels (DP-high and DP-low), the vortices originating from the tri-spoke front wheel and closed rear disk wheel (TTP) were smaller in number and size.

No significant differences could be observed between the

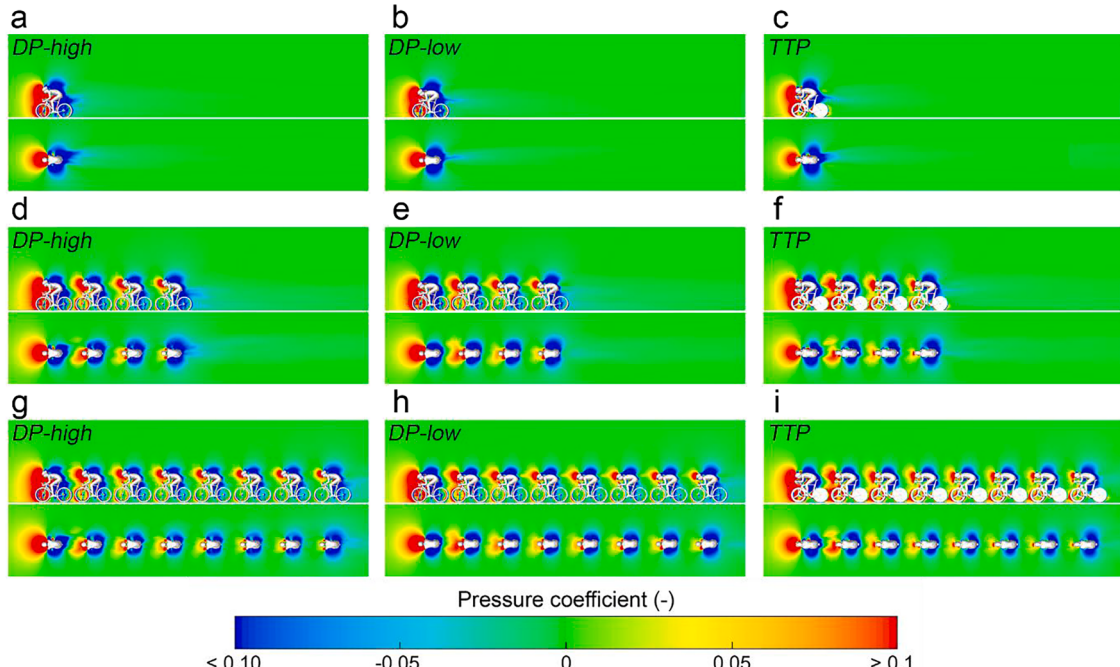


Fig. 9. Contours of mean static pressure coefficient in the vertical centerplane and in an horizontal plane at 1 m height for (a,d,g) DP-high, (b,e,h) DP-low and (c,f,i) TTP for pacelines with (a,b,c) 1, (d,e,f) 4 and (g,h,i) 8 cyclists.

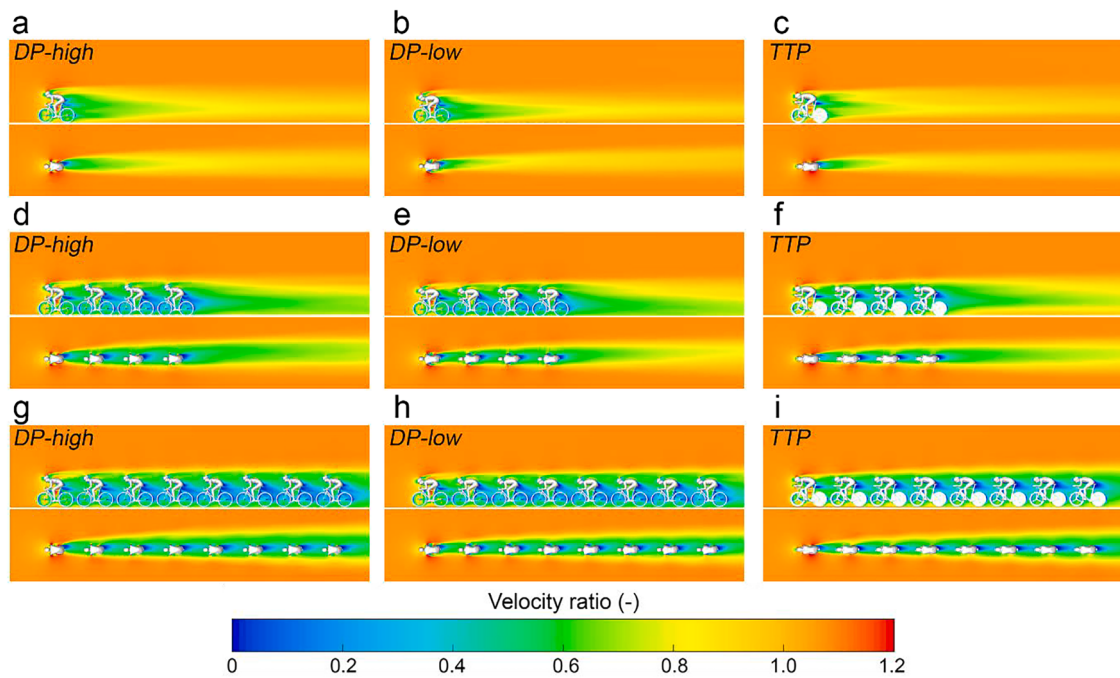


Fig. 10. Contours of mean velocity ratio in the vertical centerplane and in an horizontal plane at 1 m height for (a,b,c) DP-high, (b,e,g) DP-low and (c,f,i) TTP for pacelines with (a,b,c) 1, (d,e,f) 4 and (g,h,i) 8 cyclists.

instantaneous structures in the wake of the isolated cyclists compared to those found in the wake of the lead cyclist in the four cyclists pacelines (Fig. 12a,c,e vs. Fig. 12b,d,f). Also for the trailing cyclists the hip/thigh vortices remained the dominant wake structures. Regions with separated flow were observed in similar regions as well, but the magnitude of vorticity was reduced compared to the isolated/lead cyclist. This decrease in vorticity magnitude was larger for positions further to the back of the paceline. Figures for all pacelines are included in Appendix A.

6. Discussion

The drag of a cyclist in a single paceline can be reduced by changing posture, position, or both. With the postures studied here, a cyclist riding solo can reduce its drag area by 13% by changing from DP-high (0.266 m^2) to DP-low (0.231 m^2). This reduction is entirely attributed to change of posture. For the leading cyclist in a paceline configuration, part of the drag reduction is also attributed to subsonic upstream disturbance. In a breakaway or sprint train containing eight cyclists the drag on the leading cyclist could be reduced by 15% if all cyclists in the paceline change posture from DP-high ($\approx 0.26 \text{ m}^2$) to DP-low ($\approx 0.22 \text{ m}^2$). As one moves towards the back of the paceline, the difference in drag between successive positions reduces. This relates to the reduced growth of the core of the wake further down the paceline. In contrast to the leading cyclist, of which the drag could be greatly reduced by riding in posture DP-low, these results suggest that maintaining an aerodynamically better posture further down the paceline is less important. In addition, it is the leading cyclist who experiences most drag but also determines the pace. These results could suggest that it would be beneficial for the trailing cyclists to maintain an aerodynamically worse posture (DP-high) and thereby reduce drag on the leading cyclist due to the subsonic upstream disturbance. Because the overpressure area in front of a cyclist is larger for less aerodynamic postures, it will interact more strongly with the underpressure area behind a preceding cyclist, reducing this underpressure area and thereby the drag of the preceding cyclists. This would be in agreement with tandem cyclists, where the drag of the front cyclist could be reduced by increasing the torso angle of the rear cyclist compared to that of the front cyclist [20]. Future research could focus on

a combination of different postures within the same paceline. The mean drag area, which could be considered as a measure of traveling economy in terms of aerodynamic resistance [29] for the whole group, reduced with an increasing number of cyclists in the paceline. This was more pronounced for less aerodynamic postures. For all postures, the impact per added cyclist decreased with longer pacelines. For pacelines containing eight cyclists the mean drag area reduced to 49% (DP-high), 51% (DP-low) and 52% (TTP). This indicates that riding in pacelines of eight cyclists is about twice as efficient in terms of aerodynamic resistance compared to riding alone.

The differences in drag between the time-trial position (TTP) and the dropped positions (DP-high and DP-low) are reflected by the wake vortex structures. This is most pronounced by the regions of flow separation at the upper back and near the wheels. The cyclist in TTP was able to maintain an aerodynamically favorable posture; e.g. its frontal area was reduced by tucking its head into its shoulders. Together with its aerodynamically shaped helmet a lower head position delays flow separation at the upper back. When comparing the wake vortex structures of the isolated cyclist with the leading cyclist in the pacelines, no significant differences could be observed for all postures. Despite a significant disturbance of upstream flow, the flow structures in the wake of the trailing cyclists also hold similarity to those observed for the isolated cyclist, but with a reduced magnitude of vorticity. This corresponds with the results of Barry et al. [74], who studied flow field interactions between two cyclists. The current study shows that the magnitude of vorticity further reduces towards the back of the paceline as the number of cyclists increases.

For the investigated configurations, the position at which the minimum drag area is found is independent of cycling posture. For pacelines up to five cyclists, the lowest drag values are found for the last cyclist, while for pacelines with six, seven and eight cyclists, a minimum drag area is found at the penultimate position. This is consistent with the results of Blocken et al. [29] who used a different TTP than in the present study, but found minimum drag values at equal positions for an equal wheel-to-wheel separation distance (0.15 m).

In this study, the posture variable was isolated by scanning the same athlete for all postures and using this geometry for all positions in the paceline. While the investigated postures are common postures in race

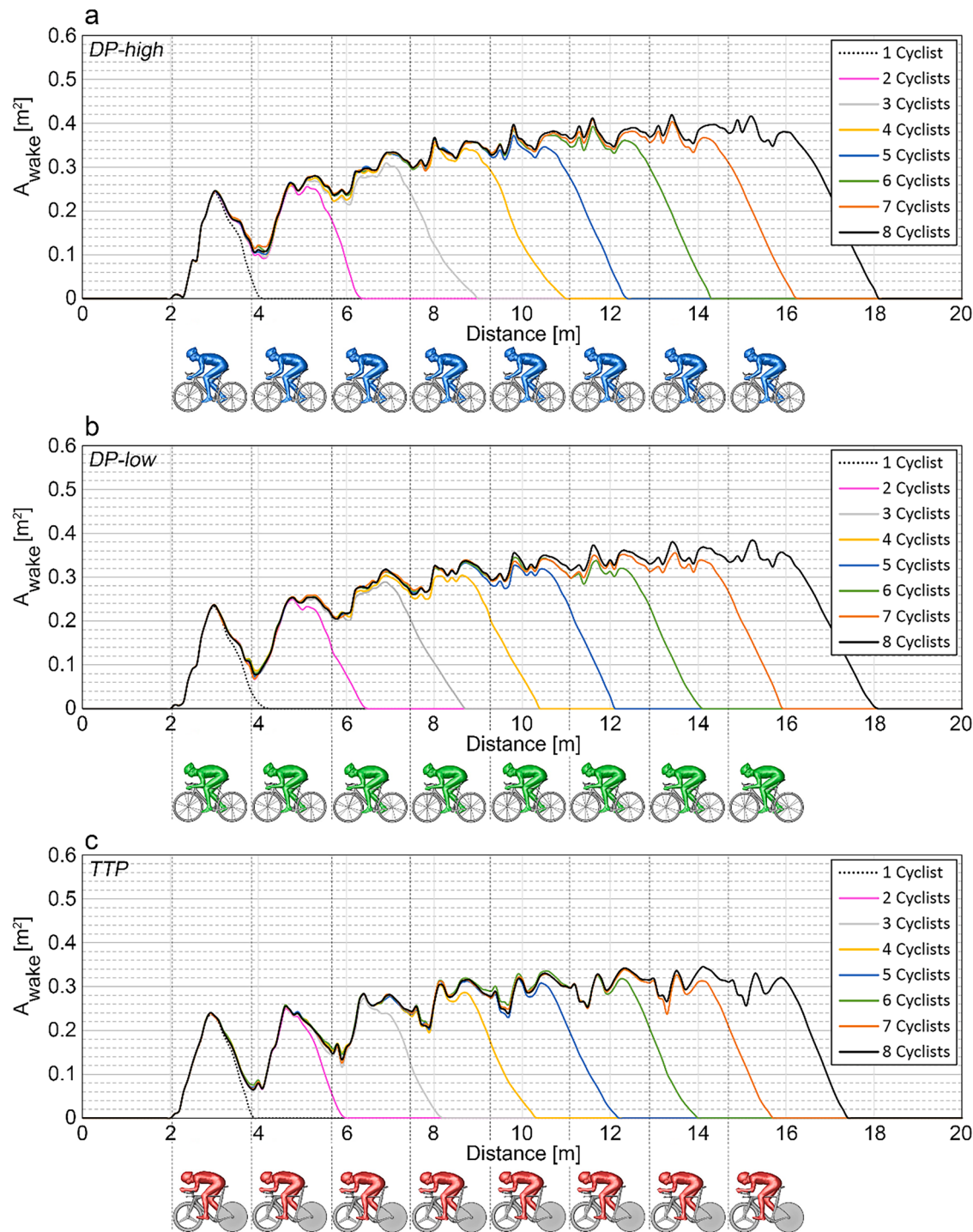


Fig. 11. Cross-sectional area of the wake (mean velocity ratio < 0.5) as a function of longitudinal distance for pacelines of up to 8 cyclists for (a) DP-high, (b) DP-low and (c) TTP.

events, in reality anthropometric differences between athletes and posture differences will impact the flow field and drag change. Future studies may use different cyclists and different cyclist postures to assess this uncertainty and test different sequences of these cyclists. An additional limitation in the present study includes the absence of crosswind effects and the bicycle wheels did not rotate. The cyclists did not pedal because this would entail additional uncertainties and higher computational costs and the time-averaged effect on the wake structure was considered to be small [59,75,76]. In agreement with previous research [77] the impact of not using a moving floor was considered negligible as

the measured boundary-layer height in the WT was well below the area of interest. Although Reynolds independence was not proven for the second cyclist, the WT measurements were considered valid for validation of the CFD simulations. Given the high geometric surface roughness on the quarter-scale model and the Reynolds number at the investigated wind speed of 25 m/s (i.e. 4×10^5), the effect of small-scale turbulence is expected to be very small and large-scale turbulence may have a greater effect on drag [78]. Fig. 12b showed that the larger structures are mainly located in front of the second cyclist. This could explain the relatively high Reynolds number sensitivity of the second

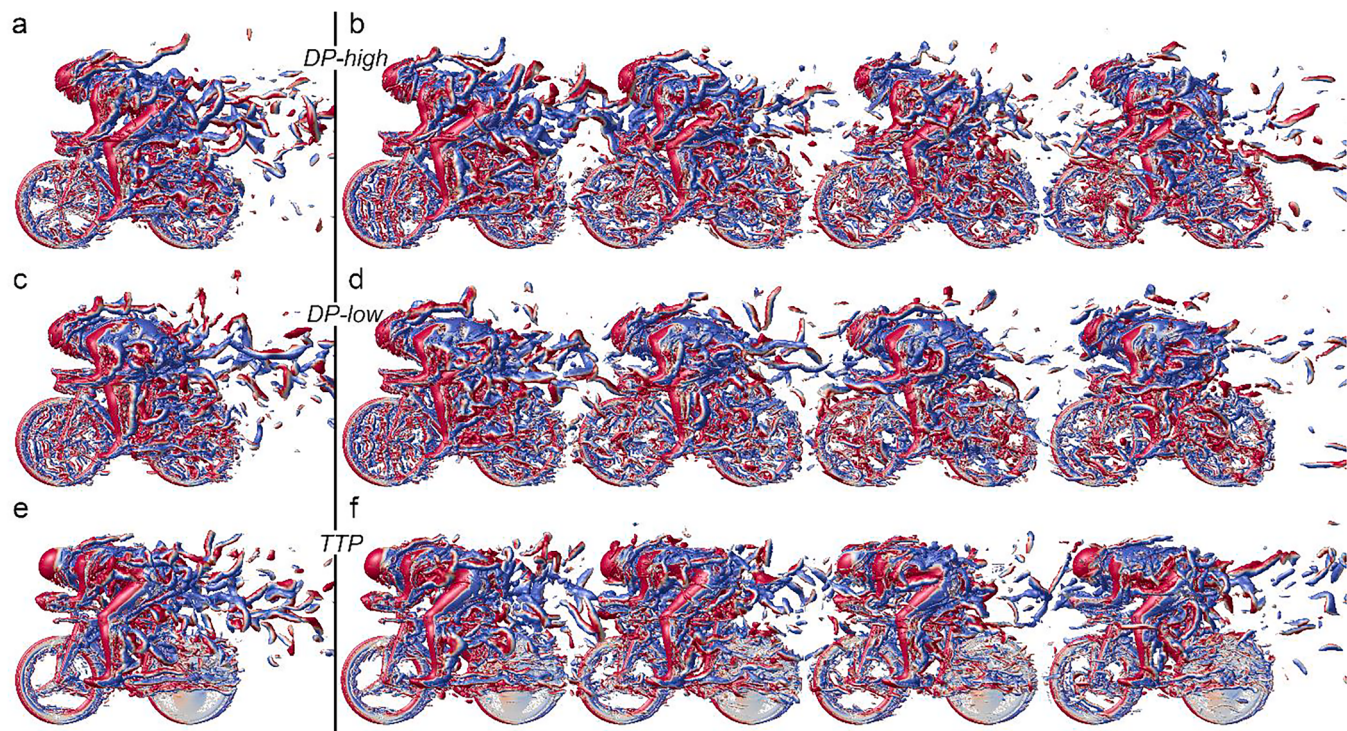


Fig. 12. Instantaneous snapshots illustrated by isosurface of q -criterion ($q = 10^3 \text{ s}^{-2}$) colored by cross-stream velocity (red-negative, blue-positive) for (a,c,e) the isolated cyclist and (b,d,f) four cyclist paceline in (a,b) DP-high, (c,d) DP-low and (e,f) TTP.

cyclist.

7. Conclusion

Although previous studies endorsed the impact of cycling postures on the effect of drafting, to the best of our knowledge, there were no systematic and extensive studies on this topic in the scientific literature. This study presented an aerodynamic analysis on the use of three different cycling postures in single paceline drafting configurations up to eight cyclists by means of WT measurements and FVM-based scale-adaptive CFD simulations. Compared to RANS methods, the scale-resolving SAS CFD method has an improved performance in wake regions, while being more robust than DES methods on complex computational grids. As the applied SAS method was based on the $k-\omega$ SST turbulence model, boundary layers flow including that in the laminar sublayer was resolved using its URANS capabilities and surface roughness could be taken into account. In addition, the application of LES would have required a very fine boundary-layer mesh in all directions and not only in the direction normal to the surface in order to resolve the whole boundary layer down to the laminar sublayer. The advantage of CFD simulations over field methods and WT testing is the ability to provide whole flow-field data, i.e. data on all computed variables in every point of the computational domain. For the isolated cyclist, the lowest drag area was obtained for the TTP (0.213 m^2). The visualized vortex structures support the obtained drag area values as there was less flow separation at the upper back and near the wheels than for DP-high and DP-low. TTP is used in individual and team time trials. In regular road races a cyclist riding solo can reduce its drag area by 13% by switching from DP-high (0.266 m^2) to DP-low (0.231 m^2).

For pacelines in which all cyclists have the same posture, the drag of a cyclist in the paceline can be reduced by changing either the posture, or the position, or both. With regard to changing posture, a drag reduction of about 15% was found for the leading cyclist in a breakaway or sprint-train when all cyclists in the paceline change from DP-high to DP-low. This drag reduction due to a change of posture reduced for

cyclists further down the pacelines. Due to the subsonic upstream disturbance, the relative drag change due to drafting with respect to riding alone is the largest for the least aerodynamic posture DP-high. This could indicate that the drag on the leading cyclist is further reduced if the trailing cyclists maintain an aerodynamically worse posture (DP-high).

In the absence of cross-wind effects the position in the paceline at which the minimum drag area was found was independent of the investigated cycling postures. In single paceline configurations up to five cyclists, the last cyclist experienced the lowest drag. In single paceline configuration of six, seven and eight cyclists, the penultimate cyclist had the lowest drag. Here, drag reductions of 63, 60 and 60% were found for DP-high, DP-Low and TTP respectively. The mean drag area reduced to 49% (DP-high), 51% (DP-low) and 52% (TTP). For all postures the longitudinal development of the core of the wake, from the first cyclist to the last cyclist in the paceline, showed a similar trend. It grew in size to position four or five in the paceline and then flattened. The magnitude of this growth is larger for less aerodynamic postures. Despite a disturbance of upstream flow, for every posture the main vortex structures in the wake of the trailing cyclists hold similarity to those observed for the isolated cyclist. However, it was shown that the magnitude of vorticity reduces as one moves further to the back of the paceline.

The maximum drag reduction was found when both the posture and the position in the paceline were changed. Compared to the isolated cyclist in DP-high posture, the cyclist could reduce its drag area by 68% by riding in penultimate position in an eight cyclist paceline in DP-low.

Funding

This work has been sponsored by NWO Exakte en Natuurwetenschappen (Physical Sciences) for the use of supercomputer facilities, with financial support from the Nederlandse Organisatie voor Wetenschappelijk Onderzoek (Netherlands Organization for Scientific Research, NWO).

Conflict of interest

The authors declare that they have no conflict of interest.

CRediT authorship contribution statement

Thijs van Druenen: Conceptualization, Validation, Investigation, Writing – original draft, Writing – review & editing, Visualization. **Bert Blocken:** Conceptualization, Writing – review & editing, Supervision.

Declaration of Competing Interest

The authors declare that they have no known competing financial interests or personal relationships that could have appeared to influence the work reported in this paper.

Data availability

The authors do not have permission to share data.

Acknowledgments

The authors acknowledge the partnership with ANSYS CFD. This work was carried out on the Dutch national e-infrastructure with the support of SURF Cooperative.

Supplementary material

Supplementary material associated with this article can be found, in the online version, at doi:<https://doi.org/10.1016/j.comfluid.2023.105863>.

References

- [1] Weimerskirch H, Martin J, Clerquin Y, Alexandre P, Jiraskova S. Energy saving in flight formation. *Nature* 2001;413:697–8. <https://doi.org/10.1038/35099670>.
- [2] Marras S, Killen SS, Lindström J, McKenzie DJ, Steffensen JF, Domenici P. Fish swimming in schools save energy regardless of their spatial position. *Behav Ecol Sociobiol* 2015;69:219–26. <https://doi.org/10.1007/s00265-014-1834-4>.
- [3] Patten, J.; McAuliffe, B.; Mayda, W.; Tanguay, B., Review of aerodynamic drag reduction devices for heavy trucks and buses, Technical Report, National Research Council Canada (2012).
- [4] Lammert M, Duran A, Dies J, Burton K, Nicholson A. Effect of platooning on fuel consumption of class 8 vehicles over a range of speeds, following distances, and mass. *SAE Int J Commer Veh* 2014;7(2):626–39. <https://doi.org/10.4271/2014-01-2438>.
- [5] Schito P, Braghin F. Numerical and experimental investigation on vehicles in Platoons. *SAE Int J Commer Veh* 2012;5(1):63–71. <https://doi.org/10.4271/2012-01-0175>.
- [6] Zabat, M.; Stabile, N.; Frascaroli, S.; Browand, F., The aerodynamic performance of Platoons: final report, technical report, California PATH project, University of California Berkeley (1995).
- [7] He M, Huo S, Hemida H, Bourriez F, Robertson FH, Soper D, Sterling M, Baker C. Detached eddy simulation of a closely running lorry platoon. *J Wind Eng Ind Aerod* 2019;193:103956. <https://doi.org/10.1016/j.jweia.2019.103956>.
- [8] Chen G, Liang X, Li X, Zhou D, Lien F, Wang J. Dynamic analysis of the effect of platoon configuration on train aerodynamic performance. *J Wind Eng Ind Aerod* 2021;211:104564. <https://doi.org/10.1016/j.jweia.2021.104564>.
- [9] Gallagher M, Mordel J, Baker C, Soper D, Quinn A, Hemida H, Sterling M. Trains in crosswinds – comparison of full-scale on-train measurements, physical model tests and CFD calculations. *J Wind Eng Ind Aerod* 2018;175:428–44. <https://doi.org/10.1016/j.jweia.2018.03.002>.
- [10] Polidori G, Legrand F, Bogard F, Madaci F, Beaumont F. Numerical investigation of the impact of Kenenisa Bekele's cooperative drafting strategy on its running power during the 2019 Berlin marathon. *J Biomech* 2020;107:109854. <https://doi.org/10.1016/j.biomech.2020.109854>.
- [11] Schickhofer L, Hanson H. Aerodynamic effects and performance improvements of running in drafting formations. *J Biomech* 2021;122:110457. <https://doi.org/10.1016/j.biomech.2021.110457>.
- [12] Bentley DJ, Libicz S, Jouglé A, Coste O, Manetta J, Chamakir K, Millet GP. The effects of exercise intensity or drafting during swimming on subsequent cycling performance in triathletes. *J Sport Sci Med* 2007;10:234–43. <https://doi.org/10.1016/j.jsams.2006.05.004>.
- [13] Beaumont F, Taiar T, Polidori G. Preliminary numerical investigation in open currents-water swimming: pressure field in the swimmer wake. *Appl Math Comput* 2017;302:48–57. <https://doi.org/10.1016/j.amc.2016.12.031>.
- [14] Spring E, Savolainen S, Erkkila J, Hamalainen T, Pihkala P. Drag area of a cross-country skier. *J Appl Biomech* 1988;4:103–13. <https://doi.org/10.1123/jjsb.4.2.103>.
- [15] Bildeau B, Roy B, Boulay MR. Effect of drafting on work intensity in classical cross-country skiing. *Int J Sports Med* 1995;16:190–5. <https://doi.org/10.1055/s-2007-972990>.
- [16] Van Ingen Schenau GJ. The influence of air friction in speed skating. *J Biomech* 1982;15:449–58. [https://doi.org/10.1016/0021-9290\(82\)90081-1](https://doi.org/10.1016/0021-9290(82)90081-1).
- [17] Rundell KW. Effects of drafting during short-track speed skating. *Med Sci Sports Exerc* 1996;28:765–71. <https://doi.org/10.1097/00005768-199606000-00016>.
- [18] Mannion P, Topalar Y, Blocken B, Hajdukiewicz M, Andrianne T, Clifford E. Improving CFD prediction of drag on Paralympic tandem athletes: influence of grid resolution and turbulence model. *Sports Eng* 2018;21(2):123–35. <https://doi.org/10.1007/s12283-017-0258-6>.
- [19] Mannion P, Topalar Y, Blocken B, Clifford E, Andrianne T, Hajdukiewicz M. Aerodynamic drag in competitive tandem para-cycling: road race versus time-trial positions. *J Wind Eng Ind Aerod* 2018;179:92–101. <https://doi.org/10.1016/j.jweia.2018.05.011>.
- [20] Mannion P, Topalar Y, Blocken B, Hajdukiewicz M, Andrianne T, Clifford E. Impact of pilot and stoker torso angles in tandem para-cycling aerodynamics. *Sports Eng* 2019;22. <https://doi.org/10.1007/s12283-019-0301-x>.
- [21] Mannion P, Topalar Y, Clifford E, Hajdukiewicz M, Andrianne T, Blocken B. On the effects of crosswinds in tandem aerodynamics: an experimental and a computational study. *Eur J Mech B Fluids* 2019;74:68–80. <https://doi.org/10.1016/j.euromechflu.2018.11.001>.
- [22] Kyle CR, Burke ER. Improving the racing bicycle. *Mech Eng* 1984;106(9):34–45.
- [23] Grappe G, Candau R, Belli A, Rouillon JD. Aerodynamic drag in field cycling with special reference to the Obree's position. *Ergonomics* 1997;40(12):1299–311. <https://doi.org/10.1080/001401397187388>.
- [24] Lukes RA, Chin SB, Haake SJ. The understanding and development of cycling aerodynamics. *Sports Eng* 2005;8:59–74. <https://doi.org/10.1007/BF02844004>.
- [25] Wilson DG. *Bicycling science*. Cambridge, MA: MIT Press; 2004.
- [26] Blocken B, van Druenen T, Topalar Y, Malizia F, Mannion P, Andrianne T, Marchal T, Maas GJ, Diepens J. Aerodynamic drag in cycling pelotons: new insights by CFD simulation and wind tunnel testing. *J Wind Eng Ind Aerod* 2018;179:319–37. <https://doi.org/10.1016/j.jweia.2018.06.011>.
- [27] Burke ER. *Serious cycling*. Champaign, IL: Human Kinetics; 2002.
- [28] Blocken B, Defraeye T, Koninckx E, Carmeliet J, Hespel P. CFD simulations of the aerodynamic drag of two drafting cyclists. *Comput Fluids* 2013;71:435–45. <https://doi.org/10.1016/j.compfluid.2012.11.012>.
- [29] Blocken B, Topalar Y, Andrianne T. Aerodynamic drag in cycling team time trials. *J Wind Eng Ind Aerod* 2018;182:128–45. <https://doi.org/10.1016/j.jweia.2018.09.015>.
- [30] Iniguez-de-la-Torre A, Iniguez J. Aerodynamics of a cycling team in a time trial: does the cyclist at the front benefit? *Eur J Phys* 2009;30:1365–9. <https://doi.org/10.1088/0143-0807/30/6/014>.
- [31] Barry N, Sheridan J, Burton D. The effect of spatial position on the aerodynamic interactions between cyclists. *Proced Eng* 2014;72:774–9. <https://doi.org/10.1016/j.proeng.2014.06.131>.
- [32] Broker JP, Kyle CR, Burke ER. Racing cyclist power requirements in the 4000-m individual and team pursuits. *Med Sci Sports Exerc* 1999;31:1677–85. <https://doi.org/10.1097/00005768-199911000-00026>.
- [33] Defraeye T, Blocken B, Koninckx E, Hespel P, Verboven P, Nicolai B, Carmeliet J. Cyclist drag in team pursuit: influence of cyclist sequence, stature, and arm spacing. *J Biomech Eng ASME* 2014;136(1):011005. <https://doi.org/10.1115/1.4025792>.
- [34] Barry N, Burton D, Sheridan J, Thompson M, Brown NAT. Aerodynamic drag interactions between cyclists in a team pursuit. *Sports Eng* 2015;18(2):93–103. <https://doi.org/10.1007/s12283-015-0172-8>.
- [35] Kyle CR. Reduction of wind resistance and power output of racing cyclists and runners travelling in groups. *Ergonomics* 1979;22(4):387–97. <https://doi.org/10.1080/00140137908924623>.
- [36] Zdravkovich, M.M.; Ashcroft, M.W.; Chisholm, S.J.; Hicks, N., Effect of cyclist's posture and vicinity of another cyclist on aerodynamic drag, Haake (Ed.), *The engineering of sport*, Balkema, Rotterdam (1996), pp. 21–28 [10.2101/9781003078098-4](https://doi.org/10.2101/9781003078098-4).
- [37] Belloli M, Giappino S, Robustelli F, Somaschini C. Drafting effect in cycling: investigation by wind tunnel tests. In: Proceedings of the 11th conference of the international sports engineering association, ISEA 2016. 147; 2016. p. 38–43. <https://doi.org/10.1016/j.proeng.2016.06.186>. Procedia Engineering.
- [38] van Druenen T, Blocken B. Aerodynamic analysis of uphill drafting in cycling. *Sports Eng* 2021;24. <https://doi.org/10.1007/s12283-021-00345-2>.
- [39] McCole SD, Claney K, Conte JC, Anderson R, Hagberg JM. Energy expenditure during bicycling. *J Appl Physiol* 1990;68:748–53. <https://doi.org/10.1152/jappl.1990.68.2.748>.
- [40] Edwards AG, Byrnes WC. Aerodynamic characteristics as determinants of the drafting effect in cycling. *Med Sci Sports Exerc* 2007;17:106–6. <https://doi.org/10.1249/01.mss.0000239400.85955.12>.
- [41] Olds T. The mathematics of breaking away and chasing in cycling. *Eur J Appl Physiol* 1998;77:492–7. <https://doi.org/10.1007/s004210050365>.
- [42] Crouch TN, Burton D, LaBry ZA, Blair KB. Riding against the wind: a review of competition cycling aerodynamics. *Sports Eng* 2017;20:81–110. <https://doi.org/10.1007/s12283-017-0234-1>.

- [43] Malizia F, Blocken B. Bicycle aerodynamics: history, state-of-the-art and future perspectives. *J Wind Eng Ind Aerod* 2020;200:104134. <https://doi.org/10.1016/j.jweia.2020.104134>.
- [44] Malizia F, Blocken B. Cyclist aerodynamics through time: better, faster, stronger. *J Wind Eng Ind Aerod* 2021;214:104673. <https://doi.org/10.1016/j.jweia.2021.104673>.
- [45] Debraux P, Grappe F, Manolova AV, Bertucci W. Aerodynamic drag in cycling: methods of assessment. *Sports Biomech* 2011;10(3):197–218. <https://doi.org/10.1080/14763141.2011.592209>.
- [46] Garcia-Lopez J, Rodriguez-Marroyo JA, Juneau CE, Peleteiro J, Cordoba Martinez A, Villa JG. Reference values and improvement of aerodynamic drag in professional cyclists. *J Sports Sci* 2008;26(3):277–86. <https://doi.org/10.1080/02640410701501697>.
- [47] Jeong W, Seong J. Comparison of effects on technical variances of computational fluid dynamics (CFD) software based on finite element and finite volume methods. *Int J Mech Sci* 2014;78:19–26. <https://doi.org/10.1016/j.ijmecsci.2013.10.017>.
- [48] Molina-Aiz FD, Fatnassi H, Boulard T, Roy JC, Valera DL. Comparison of finite element and finite volume methods for simulation of natural ventilation in greenhouses. *Comput Electron Agric* 2010;72(2):69–86. <https://doi.org/10.1016/j.compag.2010.03.002>.
- [49] ANSYS inc, ANSYS fluent - theory guide 19.2, (2018).
- [50] Weller HG, Tabor G, Jasak H, Fureby C. A tensorial approach to computational continuum mechanics using object-oriented techniques. *Comput Phys* 1998;12(6):620–31. <https://doi.org/10.1063/1.168744>.
- [51] Blocken B. 50 years of computational wind engineering: past, present and future. *J Wind Eng Ind Aerod* 2014;129:69–102. <https://doi.org/10.1016/j.jweia.2014.03.008>.
- [52] Menter FR. Eddy viscosity transport equations and their relation to the k- ϵ model. *J Fluids Eng* 1997;119:876–84. <https://doi.org/10.1115/1.2819511>.
- [53] Launder BE, Spalding DB. *Lectures in mathematical models of turbulence*. London, England: Academic Press; 1972.
- [54] Menter FR, Langtry RB, Likki SR, Suzen YB, Huang PG, Völker S. A correlation-based transition model using local variables—Part I: model formulation. *J Turbomach* 2006;128(3):413–22. <https://doi.org/10.1115/1.2184352>.
- [55] Menter FR, Langtry R, Völker S. Transition modelling for general purpose CFD codes. *Flow Turbul Combust* 2006;77(1–4):277–303. <https://doi.org/10.1007/s10494-006-9047-1>.
- [56] Blocken B, van Druenen T, Toparlar Y, Andrianne T. Aerodynamic analysis of different cyclist hill descent positions. *J Wind Eng Ind Aerod* 2018;181:27–45. <https://doi.org/10.1016/j.jweia.2018.08.010>.
- [57] Hemida H, Krajnović S. Transient simulation of the aerodynamic response of a double-deck bus in gusty winds. *ASME J Fluids Eng* 2009;131(3):031101. <https://doi.org/10.1115/1.3054288>.
- [58] Guilméneau E, Deng G, Wackers J. Numerical simulation with a DES approach for automotive flows. *J Fluids Struct* 2011;27(5):807–16. <https://doi.org/10.1016/j.jfluidstructs.2011.03.010>.
- [59] Javadi A. Aerodynamic study of the pedalling of a cyclist with a transitional hybrid RANS-LES turbulence model. *Flow Turbul Combust* 2022;108(3):717–38. <https://doi.org/10.1007/s10494-021-00297-4>.
- [60] Spalart PR. Detached-eddy simulation. *Annu Rev Fluid Mech* 2009;41(1):181–202. <https://doi.org/10.1146/annurev.fluid.010908.165130>.
- [61] Menter FR, Egorov Y. The scale-adaptive simulation method for unsteady turbulent flow predictions. Part 1 Theory Model Descr Flow Turbul Combust 2010;85(1):113–38. <https://doi.org/10.1007/S10494-010-9264-5>.
- [62] Blocken B, Malizia F, van Druenen T, Gillmeier SG. Aerodynamic benefits for a cyclist by drafting behind a motorcycle. *Sports Eng* 2020;23. <https://doi.org/10.1007/s12283-020-00332-z>.
- [63] Aultman M, Wang Z, Auza-Gutierrez R, Duan L. Evaluation of CFD methodologies for prediction of flows around simplified automotive models. *Comp Fluids* 2022; 236:105297. <https://doi.org/10.1016/j.compfluid.2021.105297>.
- [64] Artec Europe, Artec eva, 3D scanners, (2017). <https://www.artec3d.com/3d-camera/artec-eva> (accessed November 12, 2020).
- [65] Eindhoven University of Technology (2017) You tube channel; wind tunnel movie: https://www.youtube.com/watch?v=VEDn_IUJQfs.
- [66] Barlow JB, Rae WH, Pope A. *Low-speed wind tunnel testing*. 3rd edn. New York: Wiley; 1999.
- [67] Egorov Y, Menter FR, Lechner R, Cokljat D. The scale-adaptive simulation method for unsteady turbulent flow predictions. Part 2: application to complex flows. *Flow Turbul Combust* 2010;85(1):139–65. <https://doi.org/10.1007/s10494-010-9265-4>.
- [68] Kokkinakis IW, Drikakis D. Implicit large eddy simulations of weakly-compressible turbulent channel flow. *Comput Methods Appl Mech Eng* 2015;287:229–61. <https://doi.org/10.1016/j.cma.2015.01.016>.
- [69] Menter, F.R., Best practice: scale resolving simulations in ANSYS CFD. Version 2.0. <http://www.ansys.com/staticassets/ANSYS/staticassets/resourcelibrary/techbrief/f/tb-best-practices-scale-resolving-models.pdf>, 2015.
- [70] Franke, J.; Hellsten, A.; Schlüzen, H.; Carissimo, B., Best practice guideline for the CFD simulation of flows in the urban environment, COST action 732, quality assurance and improvement of microscale meteorological models, Hamburg, Germany (2007).
- [71] Tominaga Y, Mochida A, Yoshie R, Kataoka H, Nozu T, Yoshikawa M, Shirasawa T. AIJ guidelines for practical applications of CFD to pedestrian wind environment around buildings. *J Wind Eng Ind Aerod* 2008;96(10–11):1749–61. <https://doi.org/10.1016/j.jweia.2008.02.058>.
- [72] Blocken B. Computational fluid dynamics for urban physics: importance, scales, possibilities, limitations and ten tips and tricks towards accurate and reliable simulations. *Build Environ* 2015;91:219–45. <https://doi.org/10.1016/j.buildenv.2015.02.015>.
- [73] Crouch TN, Burton D, Brown NAT, Thomson MC, Sheridan J. Flow topology in the wake of a cyclist and its effect on aerodynamic drag. *J Fluid Mech* 2014;748:5–35. <https://doi.org/10.1017/jfm.2013.678>.
- [74] Barry N, Burton D, Sheridan J, Thompson M, Brown NAT. Flow field interactions between two tandem cyclists. *Exp Fluids* 2016;57:181. <https://doi.org/10.1007/s00348-016-2273-y>.
- [75] Griffith MD, Crouch TN, Burton D, Sheridan J, Brown NA, Thompson MC. A numerical model for the time-dependent wake of a pedalling cyclist. *Proc Inst Mech Eng Part P J Sports Eng Technol* 2019;233(4):514–25. <https://doi.org/10.1177/1754337119858434>.
- [76] Crouch TN, Burton D, Thomson MC, Brown NAT, Sheridan J. Dynamic leg-motion and its effect on the aerodynamic performance of cyclists. *J Fl Str* 2016;65:121–37.
- [77] Blocken B, Toparlar Y Y, Andrianne T. Aerodynamic benefit for a cyclist by a following motorcycle. *J Wind Eng Ind Aerod* 2016;155:1–10. <https://doi.org/10.1016/j.jweia.2016.04.008>.
- [78] Liu X, Levitan M, Nikitopoulos D. Wind tunnel tests for mean drag and lift coefficients on multiple circular cylinders arranged in-line. *J Wind Eng Ind Aerod* 2008;96(6–7):831–9. <https://doi.org/10.1016/j.jweia.2007.06.011>.